HANSER

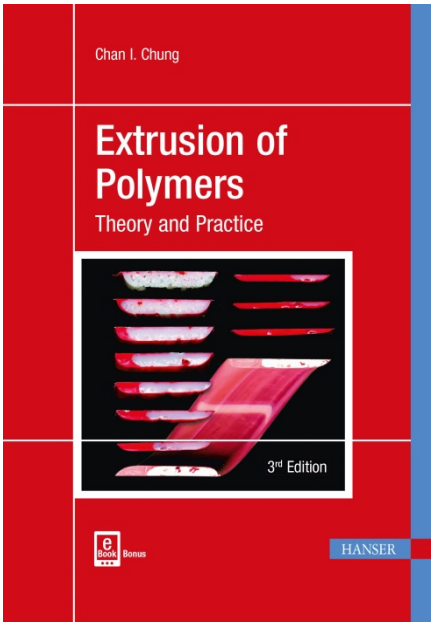

Sample Pages

Extrusion of Polymers

Chan I. Chung

ISBN (Book): 978-1-56990-609-5
ISBN (E-Book): 978-1-56990-738-2

For further information and order see

www.hanserpublications.com (in the Americas)

www.hanser-fachbuch.de (outside the Americas)

Preface

Conceptual understanding and basic analytical skill are sufficient in most cases to deal with practical engineering problems. This philosophy and the contents of this book reflect my industrial, academic, and consulting experience of over 50 years. I have been fortunate to have the opportunity to study the fundamentals of extrusion mechanisms, melt rheology, and polymer physics as well as the opportunity to apply them successfully in commercial practice. My fundamental and practical knowledge of extrusion led to several commercially successful high performance screw designs.

A process engineer must have a good knowledge of the material being processed as well as the engineering aspects of the process in order to fully understand the process and the product. This is especially true for polymers because the properties of a polymer product strongly depend on its processing history. Fundamentals of polymer physics and melt rheology are presented for those who lack previous training. This book starts at a basic level emphasizing conceptual understanding and progresses to an advanced level for ambitious readers. Theoretical models are presented with discussions on their capabilities, assumptions, and limitations. Examples show how the theoretical models can be used in practice. Discussions on disputed or ill-understood topics should be considered as my opinion.

Practical engineering problems are usually too complex to obtain exact mathematical solutions. Approximate solutions with ambiguity are obtained using simplifying assumptions and approximate material properties. The knowledge learned from practical experience is essential to properly interpret the solutions.

I wrote this book to share what I learned through my career with other engineers and scientists. I have tried to present the topics accurately, clearly, and carefully. However, mistakes and ambiguities are inevitable. Your comments will be welcome and appreciated.

Chan I. Chung

About the Author

Chan I. Chung is Professor Emeritus at Rensselaer Polytechnic Institute (RPI). Prof. Chung has been involved in polymer processing, melt rheology, and polymer physics for over 50 years; 11 years as an industrial engineer, 27 years as a professor at RPI, and the past 45 years as an active industrial consultant at numerous companies. His experience includes extrusion modeling, single-screw design, twin-screw configuration, die design, resin development, and compounding. He has authored over 100 papers and holds 12 U.S. patents. The high performance screws based on his patents have been widely used in industry for many years.

Prof. Chung was awarded the prestigious Plastics Engineering/Technology Award of the Society of Plastics Engineers (SPE) in 2004. He was made a fellow of the SPE in 1985. He received the Distinguished Service Award for outstanding contribution to the knowledge of plastics extrusion in 1987, and the Bruce Maddock Award for outstanding achievement in single-screw extrusion in 2000, both from the Extrusion Division of the SPE. Prof. Chung received his B.S. from Seoul National University, M.S. from Stevens Institute of Technology, and Ph.D. from Rutgers University.

Contents

2 Physical Description of Single-Screw Extrusion

2.1 Overall Functions of a Single-Screw Extruder

This chapter is intended to provide an overall physical understanding of the single-screw extrusion operation, including the relevant polymer properties and operating conditions. Although this chapter is quite lengthy, the reader will immediately become familiar with single-screw extrusion and develop further interests to study more details presented in the following chapters. Comprehension of the physical descriptions presented in this chapter alone may prove to be sufficiently beneficial for many readers, and help them to improve their processes and products.

Referring to Chapter 1; Fig. 1.2, an extruder is used to melt a solid polymer and deliver the molten polymer for various forming or shaping processes. The screw is the only working component of the extruder. All other components (motor, gearbox, hopper, barrel and die, etc.) merely provide the necessary support for the screw to function properly. The overall functions of an extruder are depicted below.

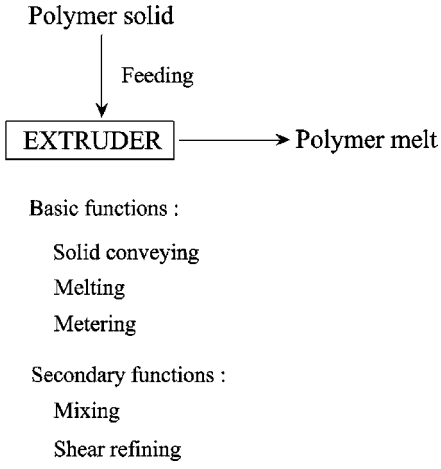

The feeding function of transferring the feed polymer from the hopper into the screw channel occurs outside of the screw, and it essentially does not depend on the screw design.

The screw performs three basic functions: (1) solid conveying function, (2) melting function, and (3) metering function or pumping function. The three screw functions occur simultaneously over most of the screw length and they are strongly interdependent. The geometric name of a screw section such as feeding section, shown in Chapter 1; Fig. 1.3, does not necessarily indicate the only function of the screw section. For example, the feeding section not only performs solid conveying function, but also melting and metering functions.

The screw also performs other secondary functions such as distributive mixing, dispersive mixing, and shear refining or homogenization. Distributive mixing refers to spacial rearrangement of different components, and dispersive mixing refers to reduction of component sizes as described in Chapter 2; Section 2.6.4. Shear refining refers to homogenization of polymer molecules by shearing.

A single-screw extruder is a continuous volumetric pump without back-mixing capability and without positive conveying capability. What goes into a screw first, comes out of the screw first. A polymer, as solid or melt, moves down the screw channel by the forces exerted on the polymer by the rotating screw and the stationary barrel. There is no mechanism to positively convey the polymer along the screw channel toward the die. The rotating screw grabs the polymer and tries to rotate the polymer with it. Suppose the barrel is removed from the extruder, or perfectly lubricated, such that it gives no resistance to the polymer movement. Then the polymer simply rotates with the screw at the same speed and nothing comes out of the screw. The stationary barrel gives a breaking force to the rotating polymer and makes the polymer slip slightly on the screw surface. The polymer still rotates with the screw rubbing on the barrel surface, but at a slightly lower speed than the screw, because of the slippage. The slippage of the polymer on the screw surface along the screw channel results in an output rate. A lubricated screw surface increases the output rate, but a lubricated barrel surface detrimentally reduces the output rate. It is clearly understandable why commercial screws are highly polished, and why grooved barrels in the feeding section are preferred. Although many commercial practices were developed empirically rather than based on theoretical analyses, they certainly agree with the underlying theoretical concepts.

The mechanisms inside a single-screw extruder are studied by examining the polymer cross-sections along the screw channel taken from “screw-freezing experiments”. In a screw-freezing experiment pioneered by Maddock [1], the screw is run to achieve a steady-state operation. Then, the screw is stopped and water cooling is applied on the barrel (and also on the screw if possible) to freeze the polymer inside the screw channel. The barrel is heated again to melt the polymer, and the screw is pushed out of the barrel as the polymer starts to melt on the barrel sur-

face. Then, the solidified polymer strip is removed from the screw channel and cut at many locations to examine the cross-sections along the screw channel. Some colored pellets are mixed in the feed to visualize the melting mechanism and the flow pattern. The colored pellets retain their shapes if they remained as solid inside the solid bed before the screw stopped, but they are sheared and become streaks inside the melt pool if they were molten before the screw stopped.

Figure 2.1 shows the cross-sections of acrylonitrile-butadiene-styrene copolymer (ABS) strip obtained from a screw-freezing experiment conducted at the Polymer Processing Technology Laboratory of The Dow Chemical Company USA. ABS pellets were extruded using a 63.5 mm (2.5 in) D, L/D = 21 conventional screw at 40 rpm. The three barrel zones from the hopper were set at 200, 230, and 250 °C, respectively. The output rate was 34.9 kg/h (77 lbs/h) at 262 °C melt temperature against 7.59 MPa (1,100 psi) head pressure.

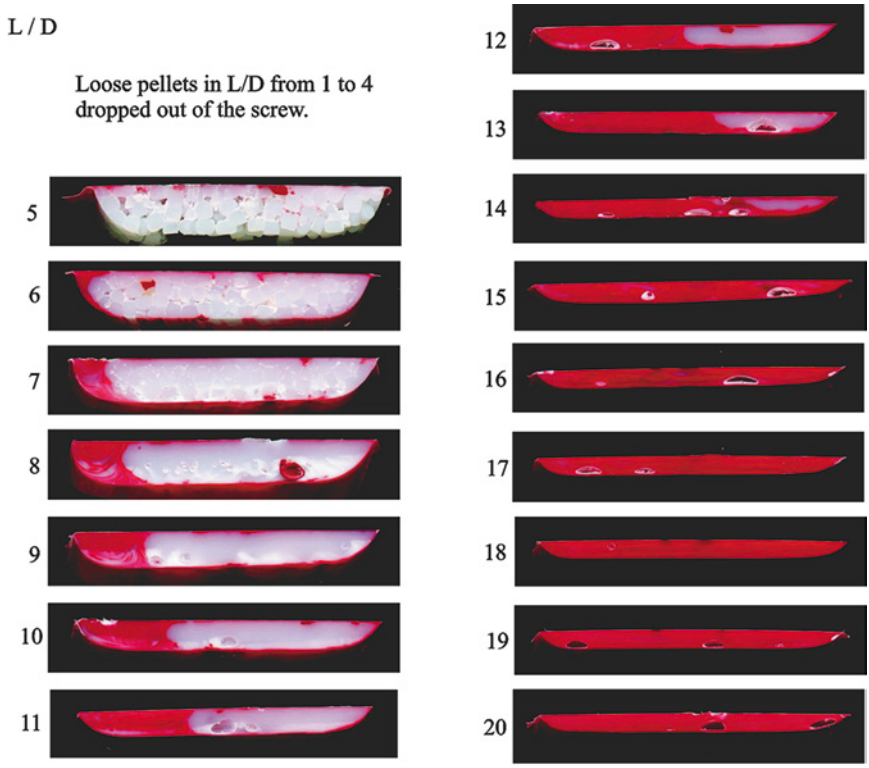

Figure 2.1 Cross-sections of ABS strip along screw channel from screw-freezing experiment (courtesy of Mark Spalding, Kun S. Hyun, and Kevin Hughes, The Dow Chemical Co. USA)

Tadmor and Klein [2], in their book, presented many examples of screw-freezing experiments. Their Fig. 5.2 for branched low density polyethylene (BLDPE) is reproduced in this book as Fig. 2.2. BLDPE pellets were extruded using a 63.5 mm (2.5 in) D, L/D = 26 conventional screw at 80 rpm. All barrel zones were set at 232 °C. The output rate was 81.5 kg/h (179.4 lbs/h) against 11.385 MPa (1,650 psi) head pressure.

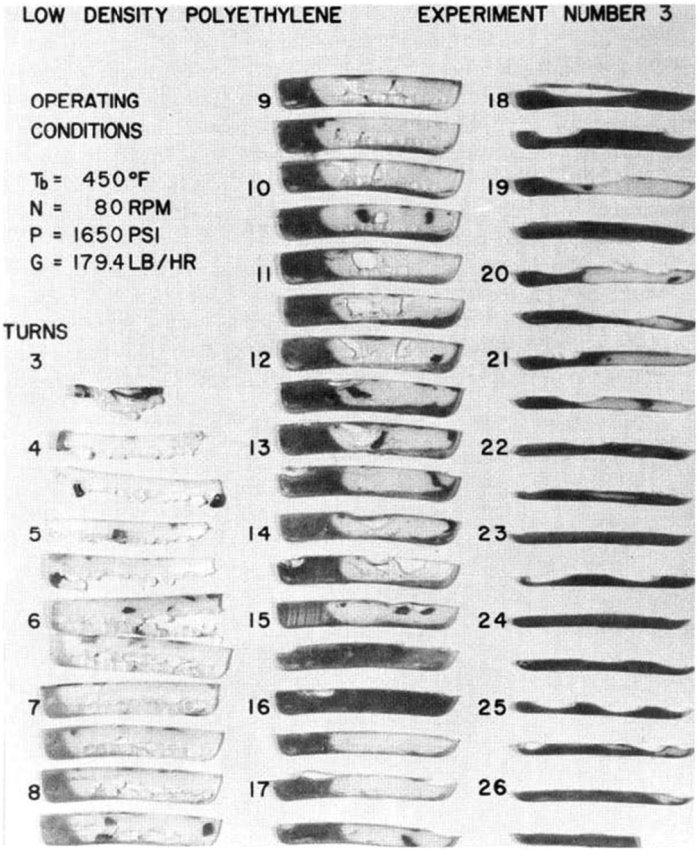

63.5 mm (2.5 in.) D., L/D = 26, extruder, running branched low density polyethylene (BLDPE) pellets.

Figure 2.2 Cross-sections of BLDPE strip along screw channel from screw-freezing experiment (reproduced from Tadmor and Klein [2])

Referring to Figs. 2.1 and 2.2, polymer pellets fed into a screw stay loose over the first 2–4 L/D of the screw from the hopper until they are compacted. Loose pellets drop out of the screw when the screw is removed from the barrel. The pellets are quickly compacted over the next 2–3 L/D into a tightly packed "solid bed". The solid bed moves down the screw channel as a rigid plug, and no mixing occurs in-

side the solid bed. The solid bed melts mainly by rubbing on the hot barrel surface as it rotates with the screw, and a thin melt film is formed on the barrel surface. The entire barrel immediately after the feed throat is set above the melting point of the polymer, unless an intensively water-cooled barrel section is used in the feeding section. The screw surface of the first several L/D is continuously cooled by cold polymer feed in a steady-state operation. The rest of the screw also becomes hot above the melting point of the polymer because of the heat conducted from hot melt. A melt film also is formed on hot screw surface, and the solid bed becomes surrounded by melt film. The thin melt film on the barrel surface is highly sheared by the rotating solid bed, and a large amount of heat is generated within the thin melt film. The thin melt film is scraped off the barrel surface and collected into a "melt pool" by the advancing flight. The melt pool is sheared and mixed as it is pumped or metered along the screw channel. The melt film on the screw surface is sheared only slightly by the slow movement of the solid bed relative to the screw, and it is not scraped off the screw surface.

The solid bed width gradually decreases and the melt pool width increases as the solid bed melts along the screw, as shown in Fig. 2.1. Melting of the solid bed is complete at about L/D = 15 in Fig. 2.1. The solid bed melts primarily by the heat conducted from the thin melt film on the barrel surface. The solid bed also melts on the hot screw surface and at the melt pool interface, but at a sufficiently lower rate to be ignored in comparison to the melting rate on the barrel surface. Melting occurs on the surface of the solid bed, and the interior of the solid bed remains virtually at the feed temperature along the screw. As the screw speed increases, the solid bed remains longer along the screw, as shown in Fig. 2.2, eventually reaching the end of the screw and causing poor melt quality. At high screw speeds, the solid bed and the melt pool coexist over most of the screw length. If the solid bed breaks up into small solid pieces before melting completely, the solid pieces become mixed with the melt pool and slowly melt by the heat conducted from the surrounding hot melt. Thus "solid bed breakup" leads to nonuniform melt temperature. Melting must be completed before the end of the screw and, preferably, the last several L/D of the screw should not contain any solid, in order to achieve uniform melt temperature.

The solid bed is strong under compression, but it can easily split under tension because the pellets in the solid bed are not fused together. The continuous solid bed strip along the screw channel will split if the front part accelerates or the rear part becomes wedged. The surrounding melt under pressure will flow into the broken area of the solid bed once the solid bed splits. Figure 2.2 clearly reveals such "solid bed splitting". The cross-sections at L/D = 16, 18.5, and also 19.5 contain only the melt without any visible solid, but the following cross-sections contain a large solid bed. Solid bed splitting causes pressure fluctuation or surging, resulting in output rate fluctuation.

Figure 2.3 is a typical segment of the solidified polymer strip in the melting section obtained from another screw-freezing experiment running ABS pellets. It shows the melt pool in front of the pushing flight and the solid bed in front of the trailing flight. The solid bed is completely surrounded by a thin melt film on both the barrel surface and the screw surface. The streaks in the melt pool show a circular flow path in the melt pool. Mixing occurs in the melt pool by the circular flow. The colored pellets in the solid bed retain their shapes, and they are not mixed at all with other pellets because the solid bed moves as a solid plug without internal deformation. The streaks on the bottom surface are the direction of the solid bed movement relative to the screw surface, and they have exactly the same helix angle as the flight because the solid bed can move down only along the screw channel. The streaks on the top surface indicate the direction of the solid bed movement relative to the barrel surface, and they have a slightly greater helix angle than the flight. The small difference, about 3° in this case, is the solid conveying angle, which is described further in Chapter 4; Section 4.2.2. The conveying rate of the solid bed, which is the same as the output rate of the extruder, depends on the solid conveying angle. A zero degree solid conveying angle corresponds to a zero output rate.

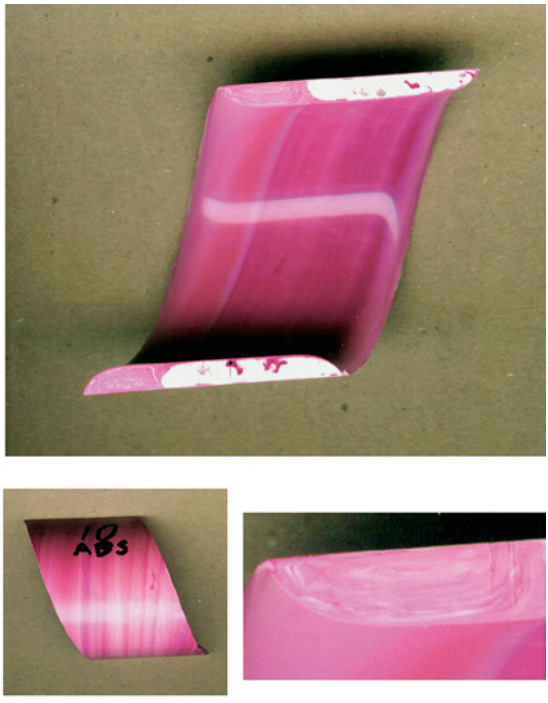

Figure 2.3 Segment of ABS strip during melting stage from screw-freezing experiment (courtesy of Kun S. Hyun and Mark Spalding, The Dow Chemical Co. USA)

toring of the operating variables and the extruder performance helps to understand the screw functions and the problems correctly, leading to optimization of the screw design and the operating conditions.

Two additional pressure measurements along the barrel, one called "P_1" at about one-third, and the other called "P_2" at about two-thirds of the barrel length from the hopper, are desired to understand what is happening inside the screw. The three pressure data, P_1, P_2, and P_h, provide diagnostic information. An unreasonably low or high value of P_1 indicates insufficient or excessive solid conveying rate, respectively. A low value of P_2 indicates insufficient supply of melt to the metering section in comparison to the pumping capability of the metering section. Severe fluctuations in P_1 or P_2 indicate inconsistent feeding, feed bridging, or wedging of the solid bed in the compression section. If the geometric compression or tapering of the screw channel in the compression section is more than the melting rate, the solid bed cannot go through the screw channel and becomes wedged temporarily until it melts enough to accommodate the geometric compression of the screw channel. If P_1 and P_2 are stable, the head pressure also should be stable.

The head pressure, measured at the end of the screw before the screen pack, slowly increases with time as the screen pack becomes clogged, slowly decreasing the output rate. The die pressure, measured at the adaptor after the screen pack, decreases as the output rate decreases. The die pressure should stay constant at a constant output rate and a constant melt temperature. A widely used feedback control slowly increases the screw rpm to maintain a constant die pressure, as the screen pack becomes clogged, assuring a constant output rate.

2.12 Rubbing Mechanisms of Solid Polymer on Metal Surface

It is well known that feed pellets are compacted into a tightly packed solid bed inside a single-screw extruder. The solid bed rotates with the screw virtually at the same velocity as the screw, rubbing and melting on the barrel surface under high pressures. The solid bed slips slightly on the screw surface as it rotates with the screw, and the slippage of the solid bed on the screw results in the output rate. The extrusion behavior of a polymer depends on the rubbing mechanisms of the solid polymer on the metal surfaces of the barrel and the screw.

Figure 2.18 shows four possible rubbing mechanisms of a solid polymer on a metal surface. At low metal temperatures below the melting (or glass transition) range of the polymer, the rubbing mechanism is "friction". Friction may occur with or without grinding the polymer. Grinding occurs if the polymer is brittle and the shear

stress τ developed between the polymer and the metal surface is high, exceeding the shear strength of the polymer. Grinding produces fine polymer powders on the metal surface, and it corresponds to a high wear mechanism. τ in friction mainly depends on pressure P. τ is proportional to P in the ideal frictional mechanism, but τ increases less than proportional to P for polymers.

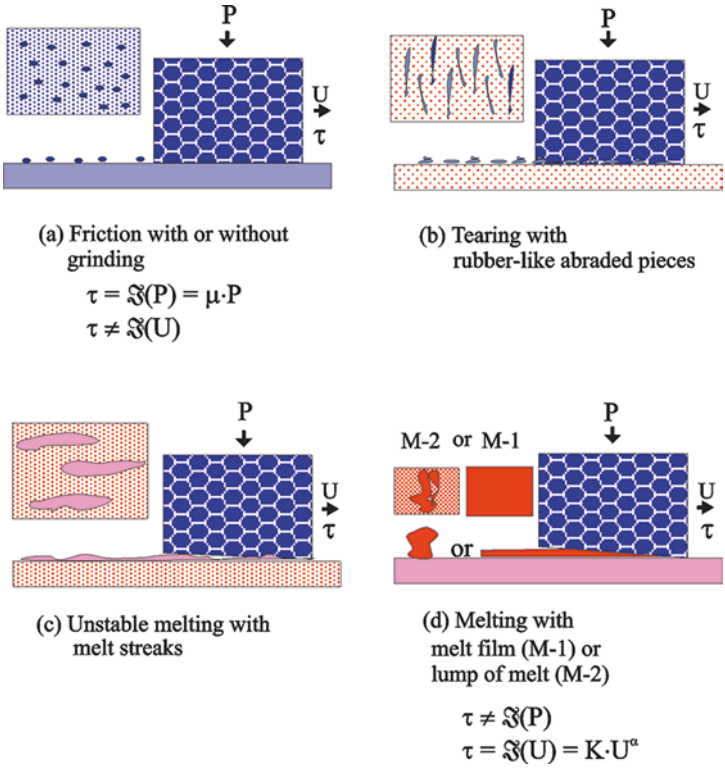

Figure 2.18 Possible rubbing mechanisms of solid polymer on metal surface

At high metal temperatures well above the melting range of the polymer, the rubbing mechanism is "melting" and a thin melt film is formed between the polymer and the metal surface. The melting mechanism forming a smooth melt film on the metal surface is denoted by M-1 in Fig. 2.18d. The melting mechanism forming lumps of the melt on the metal surface is denoted by M-2 in Fig. 2.18d. The M-2 mechanism may result from poor adhesion of melt on metal surface, high melt elasticity, or melt instability at the high shear rates in the thin melt film. The shear stress τ in the melting mechanism mainly depends on rubbing velocity (U), increasing exponentially with increasing U, similar to the dependence of melt viscosity on shear rate. Rigid, highly crystalline polymers, such as polyesters, nylons, polypropylene, and high density polyethylene, and rigid amorphous polymers

(glassy polymers), such as polystyrene and polycarbonate, make a distinct transition from the frictional mechanism to the melting mechanism with increasing metal temperature.

Soft, semi-crystalline polymers with a broad melting range, such as low density polyethylenes, exhibit intermediate rubbing mechanisms between friction and melting. “Tearing” and “unstable melting” are two representative intermediate rubbing mechanisms. Tearing occurs when the polymer at the metal temperature behaves like an elastomer, and it produces rubber-like, abraded polymer pieces on the metal surface. Unstable melting combines the tearing and melting mechanisms, producing melt streaks on the metal surface. High shear stresses are developed in tearing and unstable melting.

The rubbing mechanism of a solid polymer on a metal surface depends on the thermodynamic, mechanical, and melt rheological properties of the polymer over the temperature range from the polymer temperature to the metal temperature. These properties, in turn, depend on the molecular and morphological characteristics of the polymer.

All barrel zones of an extruder, except the first zone next to the hopper, are set at temperatures far above the melting point of the polymer in most cases, and the rubbing mechanism on the extruder barrel will be melting. The first zone is set at a lower temperature, but still well above the melting point of the polymer, to avoid the sticking problem of the feed materials on the feed throat and the screw. A barrel temperature below the start of melting mechanism, where grinding, tearing, or unstable melting mechanism occurs, should be avoided because an unnecessary high torque would be required without effectively melting the polymer.

■ 2.13 Relationships Between Screw Channel Geometries

Referring to Chapter 1; Fig. 1.3, the pitch P and the helix angle ϕ of a flight are related. Figure 2.19 shows one turn of the flight removed from the screw root and unwrapped on a flat surface. The following relationship is found:

$$\tan\phi = \frac{P}{\pi D}$$
$$\phi = \tan^{-1}\left(\frac{P}{\pi D}\right) \tag{2.13}$$

For the square-pitch with $P = D$, $\phi = 17.65°$ is found using Eq. 2.13.

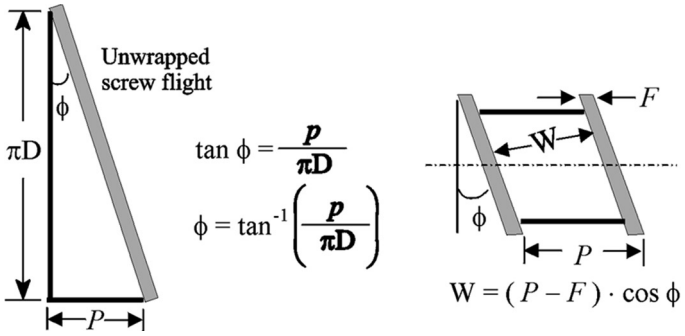

Figure 2.19 Relationships between screw channel geometries of a single-flighted screw

The cross-sectional area of the screw channel used for flow rate calculations is equal to (the channel depth H) × (the channel width W measured perpendicular to the flights). The relationship given below between the pitch P and the channel width W of a single-flighted screw is also shown in Fig. 2.19.

$$W = (P - F) \cdot \cos\phi \tag{2.14}$$

or

$$W = \pi D \cdot \sin\phi - F \cdot \cos\phi \tag{2.15}$$

where F = flight width measured along the screw axis.

■ 2.14 Variables Controlling Polymer Extrusion

The performance of an extruder for a polymer depends on polymer properties, feed characteristics, screw design parameters, and operating conditions, as discussed previously. Also, feeding conditions assuring a consistent feeding rate are essential. Table 2.1 summarizes these variables. Descriptions of the polymer properties relevant to processing are presented in Chapter 3.

Table 2.1 Variables Controlling Polymer Extrusion

Polymer properties
Thermodynamic properties
Melting characteristics – melting range
Heat capacities and thermal conductivities of solid and melt, heat of fusion
Melt rheological properties
Viscosity; elasticity; shear sensitivity; temperature sensitivity

Table 2.1 Variables Controlling Polymer Extrusion *(continued)*

Mechanical properties
Modulus; yield strength
Solid density and melt density
External friction on metal surface
Thermomechanical stability
Additives
Feed characteristics
Size and shape of feed pellets, and their distribution
Bulk density of feed pellets
Internal friction of feed pellets
Feeding conditions
Feed temperature – preheating or drying of the feed
Gravity, forced or metered (starved) feeding
Constant feeding rate, in weight
Consistent composition if more than one component feed
Recycling
Screw design parameters
Pitch (or lead)
Number of parallel flights
Feeding section depth and length
Compression (or transition) section length
Taper or reduction rate of the channel area in compression section
Metering section depth and length
Compression ratio (CR)
Mixing section design
Special channel geometry
Single or multiple stages
Operating conditions
Screw rpm
Barrel temperature settings
Head pressure
Die design; screen pack; breaker plate; adaptor
Screw temperature control

3.5.8 Elastic Memory Effect on Extrudate Shape

A polymer melt is viscoelastic with a characteristic relaxation time (see Section 3.5.1.1), and it has a memory of the stress/strain condition during a time period longer than the relaxation time after a stress/strain condition was applied. The relaxation time for a highly viscous and highly elastic polymer melt, such as high molecular weight-high density polyethylene (HMW-HDPE) and rigid polyvinyl chloride, can be very long, on the order of minutes.

The shape and layer structure, if coextruded, of an extrudate exiting a die are influenced by the previous stress/strain history leading to the die exit, and they may be quite different from the shape of the die opening or the feedblock structure [67]. Such elastic memory effect is pronounced for polymers with a long relaxation time and a large recoverable shear strain. A drastic example of the memory effect is shown in Fig. 3.46. A HMW-HDPE was fed radially into a long circular tube with 19.05 mm (0.75 in) diameter at four corners at about 18 kg/h (39.6 lbs/h). The cross-sectional shape of the extrudate exiting the circular orifice was initially circular, but it slowly changed to more or less square with four corners corresponding to the four feed ports. A picture of the final extrudate cross-section is shown. The molecules were oriented radially at the feed port and they recoil upon leaving the die, swelling at the four inlet corners.

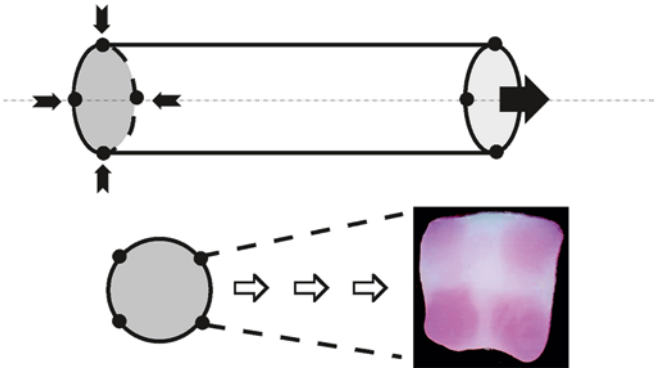

Figure 3.46 Elastic recovery of HMW-HDPE melt
Observation by C. Chung and J. Dooley at the Processing Technology Laboratory of The Dow Chemical Company USA

The elasticity of a polymer melt has pronounced effects on the flow of the polymer melt. The extrudate may show surface irregularities or distorted shapes caused by the elasticity at high extrusion speeds as discussed in Section 3.5.6. The flow through a die may develop undesirable profiles caused by the elasticity, giving incorrect extrudate shapes or structures. The elastic effects in polymer melt flow are further discussed in Chapter 8.

3.5.9 Effects of Molecular Parameters on Melt Rheological and Physical Properties

3.5.9.1 Molecular Weight (MW)

Both the melt rheological and physical properties of a polymer are correlated best to the weight average MW. Physical properties improve and viscosity increases with increasing weight average MW.

The dependence of viscosity on weight average MW for linear polymers, shown in Fig. 3.31b in Section 3.5.2.2, can be expressed by the following equation [1, 69, 70]:

$$\eta = K_T \cdot M_w^{\alpha} \tag{3.89}$$

where

η = viscosity of a polymer melt

M_w = weight average molecular weight

K_T = temperature-dependent constant

α = 1.0 for $M_w < M_c$

α = 3.4 for $M_w > M_c$ at zero shear rate, decreasing to 1.0 at infinite shear rate

M_c is the critical MW for entanglement, and its value depends on the polymer. It is noted again that Eq. 3.89 is applicable only to linear polymers.

The relationship between viscosity and MW for branched polymers is not completely developed. The following equation is proposed for branched low density polyethylene [13, 68]:

$$\eta = L_T \cdot (M \cdot g)_w^{\beta} \tag{3.90}$$

where

M = molecular weight

g = branching parameter < 1.0, defined by the ratio of the radii of gyration of branched molecule to linear molecule with the same MW

$(M \cdot g)_w$ = weight average of $(M \cdot g)$ of all molecules

L_T = temperature-dependent constant

The uncertainty of Eq. 3.90 arises from the high experimental value of $\beta = 6.6–6.8$ at zero shear rate [13, 68], which is about twice of $\alpha \approx 3.4$ for linear polymers.

The shear sensitivity of viscosity increases with increasing MW. However, the temperature sensitivity of viscosity or the apparent flow activation energy does not depend on MW for commercial polymers with high MWs (see Section 3.5.2.3).

Measured at a constant shear stress, the recoverable shear strain or extrudate swell ratio of a polymer melt increases with increasing MW at low MW, but becomes constant above a very high MW that is much higher than the critical MW for entanglement [69]. However, the shear stress measured at a constant shear rate

continuously increases with increasing MW because the viscosity increases with MW. Consequently, the recoverable shear strain measured at a constant shear rate continuously increases with increasing MW.

3.5.9.2 Molecular Weight Distribution (MWD)

The MWD or polydispersity of a polymer is usually defined by the ratio of weight average MW to number average MW (see Section 3.2.2). Broader MWD indicates more low MW molecules and more high MW molecules. MWD strongly influences the shear thinning behavior and the elasticity of a polymer melt [3, 69, 70] as well as the physical properties. Physical properties generally deteriorate with increasing MWD at the same weight average MW because of the weakness of low MW molecules.

The effect of MWD on shear thinning behavior is shown in Fig. 3.47 for two polymers with the same weight average MW or [MI]. The polymer with broad MWD starts the shear thinning behavior at a lower shear rate than a polymer with narrow MWD. For the usual processing range of shear rate, the polymer with broad MWD is more shear thinning than the polymer with narrow MWD. When two polymers with the same [MI] are compared, the one with broader MWD will have lower viscosity at the high shear rates of processing, consuming less torque and developing lower melt temperature.

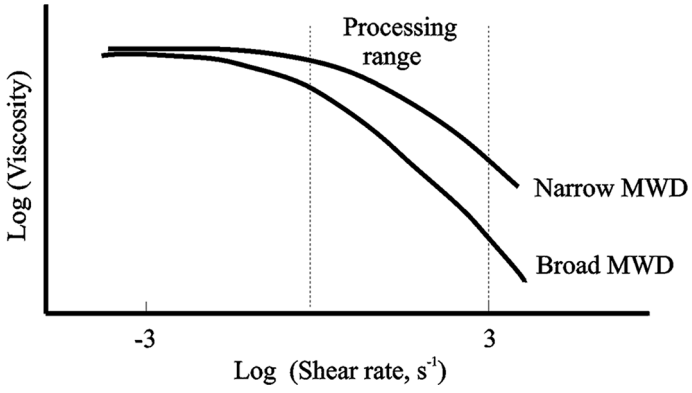

Figure 3.47 Dependence of shear sensitivity on molecular weight distribution

The apparent flow activation energies of commercial polymers with high MWs does not depend on MWD because apparent flow activation energy is independent of MW at high MWs.

The recoverable shear strain or extrudate swell ratio of a polymer melt is affected more by high MW molecules than low MW molecules, and it is sensitive to the z-average MW. The extrudate swell ratio can be significantly increased by a small

amount of very high MW molecules. Measured at a constant shear stress, the extrudate swell ratio increases with increasing MWD.

3.5.9.3 Molecular Structure

The physical and the melt rheological properties of a polymer as well as the morphology of the polymer strongly depend on the molecular structure. Various polyethylenes with different molecular structures, shown in Fig. 3.48, are widely used, and they provide an excellent example to study the effects of molecular structure [5].

A perfect polyethylene (PE) crystal with orthorhombic unit cell structure has 0.9972 g/cm^3 density at 30 °C with a melting point at about 141 °C [71], and it is a hard solid at room temperature (RT). Amorphous PE has 0.855 g/cm^3 at 30 °C [71] with a glass transition temperature at about −120 °C, and it behaves as a soft elastomer at RT. PE molecules cannot crystallize completely because of structural irregularities such as chain ends, short chain branches (SCB), and long chain branches (LCB), as well as the chain folding behavior. A branch is considered a LCB if it has a sufficiently long length for entanglement. The crystallinity decreases as the amount of SCB or LCB increases, resulting in a lower density and a lower modulus.

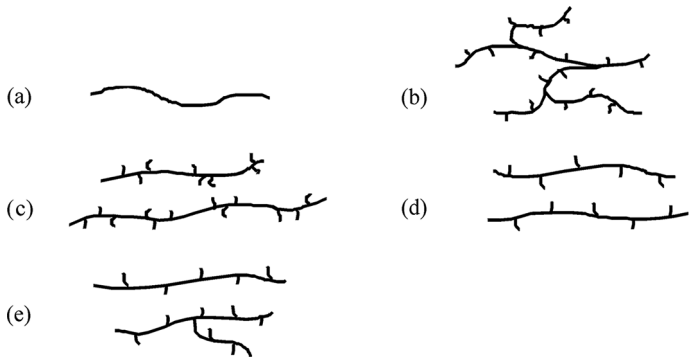

Figure 3.48 Molecular Structures of Various Polyethylenes: (a) Linear or high density polyethylene (HDPE); (b) Branched low density polyethylene (BLDPE); (c) Ziegler-Natta or heterogeneous linear low density polyethylene; (d) Metallocene or homogeneous linear low density polyethylene; (e) Homogeneous linear low density polyethylene with occasional long chain branches

High density polyethylene (HDPE), shown in Fig. 3.48a, is a homopolymer of ethylene with a linear molecular structure. HDPE crystallizes to a high degree, reaching about 80 wt.% crystallinity, resulting in a high density around 0.950 g/cm^3, as the name indicates.

4.2.3 Analysis of the Solid Conveying Angle

A small segment of a solid bed with a segmental length ΔZ along the screw channel is shown in Fig. 4.7, together with various forces acting on the solid bed segment. These forces and the resulting torque are at equilibrium and control the movement of the solid bed segment relative to the barrel and the screw. It is a three-body dynamic problem with a stationary barrel, a rotating screw, and a floating solid bed. The movement of the solid bed relative to the screw, that is, the slippage of the solid bed on the screw, results in solid conveying.

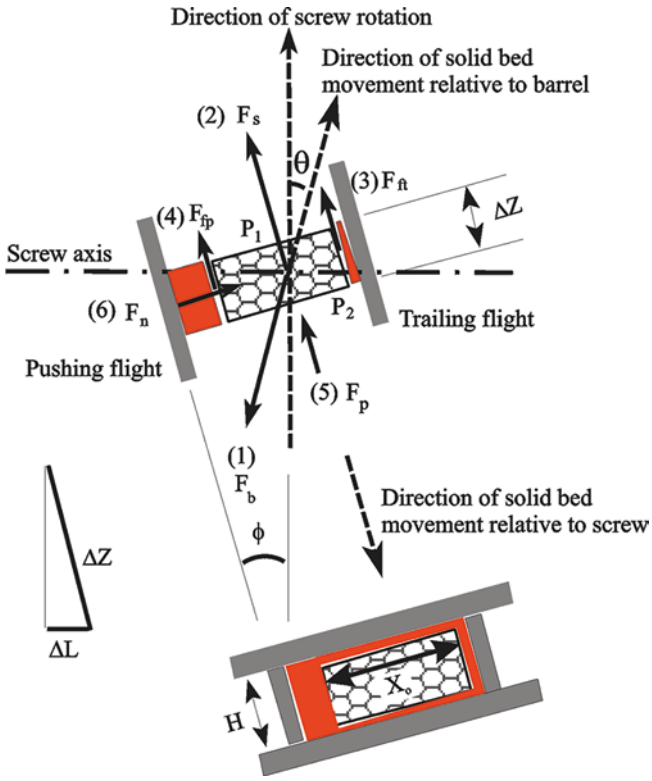

Figure 4.7 Segment of solid bed in melting section and six forces acting on the segment: (1) Force on the barrel; (2) Force on the screw root; (3) Force on the trailing side of the flight; (4) Force on the pushing side of the flight; (5) Force caused by the pressure; (6) Kinetic force on the pushing side of the flight

There are six forces acting on the solid bed segment:

1. F_b is the force on the barrel resisting the solid bed movement on the barrel in the θ-direction. This force acts in the negative θ-direction at a distance R from the screw axis.

2. F_s is the force on the screw root resisting the movement of the solid bed relative to the screw. This force acts in the screw channel ϕ-direction toward the hopper at a distance (R − H) from the screw axis.
3. F_{ft} is the force on the trailing side of the flight resisting the movement of the solid bed relative to the screw. This force acts in the screw channel ϕ-direction toward the hopper at an average distance (R − ½H) from the screw axis.
4. F_{fp} is the force on the pushing side of the flight resisting the movement of the solid bed relative to the screw. This force acts in the screw channel ϕ-direction toward the hopper at an average distance (R − ½H) from the screw axis.
5. F_p is the force caused by the pressure increase along the screw channel. This force pushes the solid bed segment in the screw channel ϕ-direction toward the hopper at an average distance (R − ½H) from the screw axis.
6. F_n is the kinetic force acting on the solid bed segment by the pushing flight in the direction perpendicular to the pushing flight. This force acts at an average distance (R − ½H) from the screw axis.

The above six forces must be at equilibrium in a steady-state operation, canceling out each other without any residual force or torque. Referring to Fig. 4.7, the solid conveying angle θ in a steady-state operation is calculated from the dynamic equilibrium force and torque balances among the various forces acting on the solid bed segment.

Taking the die direction as positive, the force balance along the screw axis is

$$-F_b \cdot \sin\theta - (F_s + F_{fp} + F_{ft} + F_p) \cdot \sin\phi + F_n \cdot \cos\phi = 0 \tag{4.8}$$

The torque balance in the direction of screw rotation is

$$-F_b \cdot \cos\theta \cdot R + F_s \cdot \cos\phi \cdot (R - H) + (F_{fp} + F_{ft} + F_p) \cdot \cos\phi \cdot \left(R - \frac{1}{2}H\right) + F_n \cdot \sin\phi \cdot \left(R - \frac{1}{2}H\right) = 0 \tag{4.9}$$

F_b, F_s, F_{fp}, and F_{ft} are the shear forces, and they can be expressed in terms of the corresponding shear stress and acting area.

$$F_b = \tau_b \cdot X_o \cdot \Delta Z_b \tag{4.10}$$

$$F_{ft} = \tau_{ft} \cdot H \cdot \Delta Z \tag{4.11}$$

$$F_s = \tau_s \cdot X_o \cdot \Delta Z_s \tag{4.12}$$

$$F_{fp} = \tau_{fp} \cdot H \cdot \Delta Z \tag{4.13}$$

Referring to Fig. 4.6, the length of the solid bed segment measured along the screw channel is ΔZ_b on the barrel surface and ΔZ_s on the screw root because of the curvature of the screw channel. The average length of the solid bed segment is

$$\Delta Z = \frac{1}{2}(\Delta Z_b + \Delta Z_s) \tag{4.14}$$

F_p is caused by the increased pressure $\Delta P = P_2 - P_1$ along the solid bed segment, and it can be expressed as

$$F_p = \Delta P \cdot X_o \cdot H \tag{4.15}$$

P_1 and P_2 are the average pressure in the screw channel at Z_1 and Z_2, respectively. It is possible that the pressure varies across the screw channel at a given Z.

The reduced channel depth k is defined by

$$k = \frac{H}{R} \tag{4.16}$$

The following dimensionless geometric constants are defined to simplify the equations, and they are further related to k using the geometry of the screw channel.

$$C_1 = \frac{\Delta Z_b}{\Delta Z} = \frac{R}{\left(R - \frac{1}{2}H\right)} = \frac{1}{\left(1 - \frac{1}{2}k\right)} \tag{4.17}$$

$$C_2 = \frac{\Delta Z_s}{\Delta Z} = \frac{(R - H)}{\left(R - \frac{1}{2}H\right)} = \frac{(1 - k)}{\left(1 - \frac{1}{2}k\right)} \tag{4.18}$$

C_1 and C_2 are close to unity for large screws with negligible channel curvature or very shallow screw channel with $H << R$. Substituting Eqs. 4.10 to 4.18 into Eqs. 4.8 and 4.9, and further eliminating the elusive kinetic force F_n by combining the resulting equations, the following equation is obtained:

$$\frac{\Delta P}{\Delta Z} = \frac{C_1}{H} \cdot \tau_b \cdot (C_1 \cdot \cos\theta \cdot \cos\phi - \sin\theta \cdot \sin\phi) - \frac{C_2}{H} \cdot \tau_s \cdot (\sin^2\phi + C_2 \cdot \cos^2\phi) - \frac{1}{X_o}(\tau_{fp} + \tau_{ft}) \tag{4.19}$$

It is noted that $\cos\theta$ decreases and $\sin\theta$ increases almost proportionally to θ as θ increases for small values of θ in the range of 2–5° found for actual extrusion operations.

There are two interdependent unknowns in Eq. 4.19:

1. Pressure gradient, $\Delta P / \Delta Z$
2. Solid conveying angle, θ

One of them must be known or assumed to calculate the other. Eq. 4.19 was derived without making any assumption crucial to its validity. Eq. 4.19 is in a simple format, and several important points can be learned for the effects of operating conditions and screw design on the solid conveying rate by examining this simple equation. The most important point is that, for a given pressure gradient along the screw, the solid conveying angle (i.e., the solid conveying rate) increases as the shear stress on the barrel (τ_b) increases or as the shear stress on the screw (τ_s) decreases, as shown in Fig. 4.8.

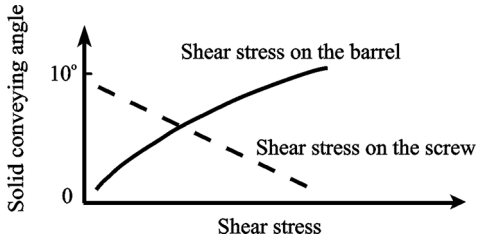

Figure 4.8 Solid conveying angle as a function of the shear stress acting on barrel or the shear stress acting on screw

4.2.4 Solid Conveying Model Based on Viscosity

All barrel zones starting immediately after the throat section are set well above the melting point of a polymer in most cases, and the solid bed is surrounded by the melt film and the melt pool, as shown in Chapter 2; Figs. 2.6, and Figs. 4.1 and 4.7. The forces acting between the solid bed and the surrounding hot metal surfaces are viscous shear forces. A solid bed conveying model for this situation was developed by Chung [1].

The following six assumptions and simplifications are made in Chung's model based on viscosity:

1. The solid bed is surrounded by melt film on all four sides: the barrel, the screw root, the pushing side, and the trailing side of the flight.
2. The solid bed moves along the screw channel as a solid plug, and the stresses involved in internal deformation of the solid bed are ignored.
3. The internal pressure of the solid bed changes only along the screw channel.
4. There is a kinetic force F_n acting on the pushing flight resulting from the advancing movement.
5. The slight difference in the helix angle of the flight from the bottom to the top of the flight is neglected.
6. The clearance between the flight and the barrel is negligible.

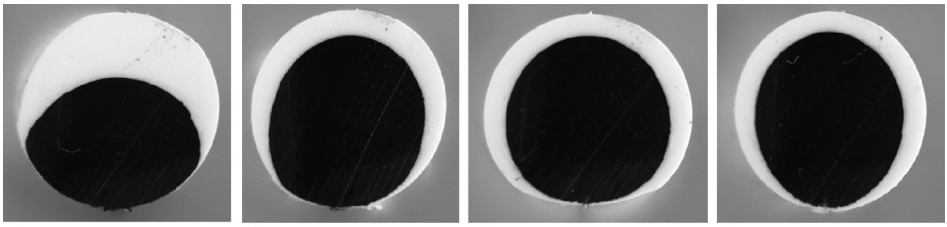

Figure 8.7 Layer interface deformation for a coextruded structure of polyethylene A resin in the cap layer and polyethylene D resin in the substrate layer flowing through a circular channel. Section (a) is from near the entry of the channel while section (d) is from near the exit of the channel

■ 8.4 Elastically Driven Flows

The previous section described how differences in viscosities in different layers in a multilayered structure can produce a flow field that leads to "viscous encapsulation" that produces layer non-uniformities. This section will cover elastic effects in polymer melt flow and how they produce different flow patterns that can also affect layer uniformity in coextruded structures.

8.4.1 Background and Theory

It has been shown previously that non-Newtonian flows in a straight pipe of non-circular cross-section are subject to secondary recirculations, with velocity components orthogonal to the primary axial flow. When a non-Newtonian fluid is sheared, it may experience two normal stress differences:

$$N_1(\dot{\gamma}) = \tau_{11} - \tau_{22} = \Psi_1(\dot{\gamma})\dot{\gamma}^2 \tag{8.1}$$

$$N_2(\dot{\gamma}) = \tau_{22} - \tau_{33} = \Psi_2(\dot{\gamma})\dot{\gamma}^2 \tag{8.2}$$

where $\dot{\gamma}$ is the shear rate and Ψ_1 and Ψ_2 are the first and second normal stress coefficients.

Directions 1, 2, and 3 are the flow, velocity gradient, and the neutral directions, respectively [20]. The stress components in the transverse plane are ultimately responsible for the secondary flow. But geometry plays a key role as well, and no secondary flow occurs in a circular pipe. The normal stresses are usually said to represent fluid "elasticity", even though they actually stem from the nonlinearity of the constitutive equation and do not imply an elastic relaxation time. Although the magnitude of viscoelastic secondary flow is typically orders of magnitude lower

than the primary flow, it may produce significant effects by introducing flow across the otherwise rectilinear streamlines. For example, it is known to greatly enhance heat transfer in pipe flows [21, 22]. In bicomponent coextrusion, secondary flows produce considerable interface deformation over an axial distance ≈ 100 D, D being the characteristic dimension of the cross-section [23–27].

Because of its fundamental and practical importance, the secondary flow of non-Newtonian fluids in non-circular pipes has received numerous investigations since the 1950s. Experimentally, several groups have observed secondary flows of polymer solutions and melts in pipes of elliptic [28] and square cross-sections [23, 24, 26, 27, 29, 30]. For an elliptic cross-section, four recirculation areas occupy the four symmetric quadrants, flowing from the center toward the wall along the minor axis and back to the center along the major axis. For a square cross-section, eight recirculation areas are demarcated by the symmetry lines, going from the center of the sides toward the corners. Theoretically and computationally, a larger number of studies have been devoted to secondary flows in those geometries, using different constitutive models: Reiner-Rivlin [21, 28, 31, 32], Criminale-Ericksen-Filbey (CEF) [22, 29, 30, 33, 34], co-rotational Maxwell [35], Phan-Thien-Tanner (PTT) [36], modified PTT (MPTT) [37], Giesekus [25, 27], and Leonov [38]. For square and elliptic cross-sections, all predict the correct number of recirculation zones and the general flow pattern.

8.4.2 Numerical Simulations

The momentum and continuity equations for the steady-state flow of an incompressible viscoelastic fluid are given by

$$-\nabla p + \nabla \cdot \mathbf{T} = 0 \tag{8.3}$$

$$\nabla \cdot \nu = 0 \tag{8.4}$$

where p is the pressure field, $\mathbf{T}$ is the viscoelastic extra-stress tensor, and ν is the velocity field.

Inertial and volume forces are assumed to be negligible.

If a discrete spectrum of N relaxation times is used, then $\mathbf{T}$ can be decomposed as follows:

$$\mathbf{T} = \sum_{i=1}^{N} \mathbf{T}_i \tag{8.5}$$

where $\mathbf{T}_i$ is the contribution of the i-th relaxation time to the viscoelastic extra-stress tensor.

For the extra-stress tensor $\mathbf{T}_i$, a constitutive equation must be chosen. For example, the Giesekus constitutive equation takes the form

$$\mathbf{T}_i\left[\mathbf{I}+\frac{\alpha_i\lambda_i}{\eta_i}\mathbf{T}_i\right]+\lambda_i\overset{\nabla}{\mathbf{T}}_i=2\eta_i\mathbf{D} \tag{8.6}$$

where $\mathbf{I}$ is the unit tensor, λ_i are the relaxation times, η_i are the partial viscosity factors, $\mathbf{D}$ is the rate of deformation tensor, and the symbol ∇ stands for the upper-convected time derivative operator.

In Equation 8.6, α_i are additional material parameters of the model, which control the ratio of the second to the first normal stress difference. In particular, for low shear rates, $\alpha_1 = -2\ N_2/N_1$, where α_1 is associated with the highest relaxation times λ_i.

The rate of deformation tensor $\mathbf{D}$ can be written as:

$$\mathbf{D}=\frac{1}{2}\left(\nabla\mathrm{v}+\nabla\mathrm{v}^{\mathrm{T}}\right) \tag{8.7}$$

The finite element technique was used to solve the set of equations described. Depending on the number of relaxation times used, the computational resources required to solve the problem can be extremely large. When more than a single relaxation time was required, the elastic viscous split stress (EVSS) algorithm was used. This method divides the viscoelastic extra stress tensor into elastic and viscous parts as follows:

$$\mathbf{T}_i=\mathbf{S}_i+2\eta_i\mathbf{D} \tag{8.8}$$

Using this algorithm, the equations expressed in terms of $\mathbf{S}_i$, $\mathbf{D}$, v, and p can be solved. A post-calculation then gives the total viscoelastic extra-stress tensor $\mathbf{T}$. A quadratic interpolation is used for v, while a linear interpolation is used for $\mathbf{S}_i$, $\mathbf{D}$, and p.

The numerical simulations of the flow of the polystyrene resin in this study were performed using a Giesekus model with five relaxation times. Figure 8.8 shows the secondary flow patterns predicted by the simulation for flow in the square channel. Because of the symmetry of the channel shape, there are two secondary flow patterns in each quadrant resulting in a total of eight secondary flow zones.

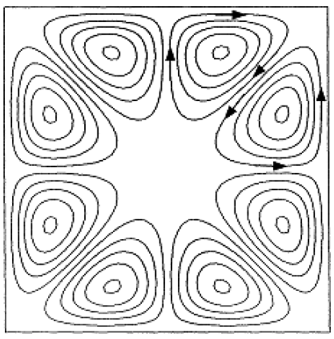

Figure 8.8 Simulation results for square channel

Figure 8.9 shows the results from a similar simulation using the triangular channel rather than the square channel. Note that the symmetry of this geometry produces a total of six secondary flow zones compared to the eight seen in the square channel.

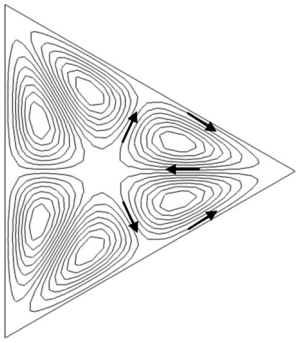

Figure 8.9 Simulation results for triangular channel

One common misconception is that the secondary flows observed in the square and triangular channels are due to the sharp corners present in these geometries. In actuality, the secondary flows are caused by second normal stress differences produced in non-radially symmetric geometries. This implies that flow through a non-radially symmetric geometry with no corners, such as an oval, would still produce secondary flows. This result is illustrated in Fig. 8.10 showing the predicted secondary flow patterns in an oval channel. Note that there are only four secondary flow regions in this geometry.

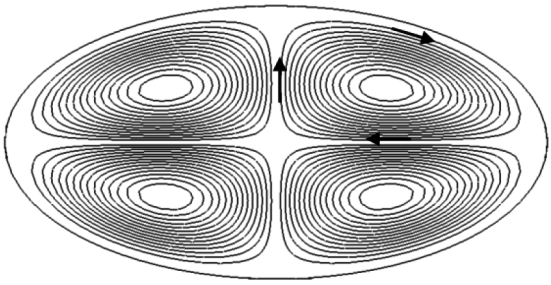

Figure 8.10 Simulation results for oval channel

Figure 8.11 shows the simulation results for a rectangular channel with 4:1 aspect ratio. These results are similar to the results from the square channel since there are eight total secondary flow areas (two per quadrant). The results are different from the square channel, however, because the strength and location of the sec-

ondary flow areas have changed. Note that the secondary flow areas near the short channel wall are much smaller than those near the long channel wall.

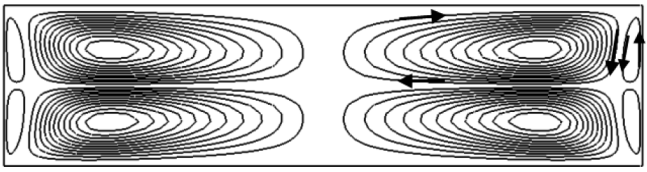

Figure 8.11 Simulation results for rectangular channel

Figure 8.12 shows the simulation results for a rectangular channel in which one end has been rounded into a semi-circular shape. These results show that rounding one end of the rectangular channel has eliminated two of the secondary flow areas, reducing the total number from eight to six.

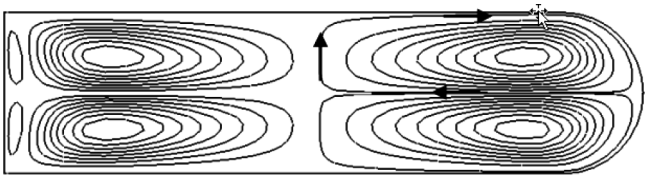

Figure 8.12 Simulation results for rounded rectangular channel

8.4.3 Experimental Procedures

The resin chosen for this study was a high impact polystyrene resin manufactured by The Dow Chemical Company. The rheological properties of this resin have been described previously [24]. This resin was chosen because it has exhibited significant viscoelastic properties in previous studies.

The equipment and experimental procedures used in these experiments were the same as those described previously in Section 8.3. The normal extrusion rate was approximately 2.5 kg/h for the polystyrene resin at 200 °C, which would give a wall shear rate of approximately 10 s^{-1}.

The first major difference in these experiments was that an identical polymer was used in the individual layers such that all the layers had the same viscosity. Thus, the viscous encapsulation phenomenon would be minimized and only the elastic effects would be present.

The second major difference was that the feedblocks were designed to produce specific coextruded structures with alternating layers or strands of the same polystyrene pigmented black or white. A series of experiments were conducted that

Author Index

Subject Index

D

E

F

G

H

I

K

L

M

N

O

P

Q

R

S

T

U

V

W

X

Z